Bidecadal temperature anomalies over the Tibetan Plateau and Arctic in response to the 1450s volcanic eruptions

Wei Liu[1,2], Feng Shi[2,3,*], Guoqiao Xiao[1], Huihong Xue[2,4], Qiuzhen Yin[5], Fei Liu[6], Anmin Duan[7], Cunde Xiao[8], Zhengtang Guo[2,3,4]

[1] School of Geography and Information Engineering, China University of Geosciences (Wuhan), Wuhan 430074, China.

[2] Key Laboratory of Cenozoic Geology and Environment, Institute of Geology and Geophysics, Chinese Academy of Sciences, Beijing 100029, China.

[3] Center for Excellence in Life and Paleoenvironment, Chinese Academy of Sciences, Beijing 100044, China.

[4] College of Earth and Planetary Sciences, University of Chinese Academy of Sciences, Beijing 100049, China.

[5] Georges Lemaître Centre for Earth and Climate Research, Earth and Life Institute, Université Catholique de Louvain, Louvain-la-Neuve, Belgium.

[6] School of Atmospheric Sciences Sun Yat-Sen University, Key Laboratory of Tropical Atmosphere-Ocean System Ministry of Education, and Southern Marine Science and Engineering Guangdong Laboratory, Zhuhai 519082, China.

[7] State Key Laboratory of Numerical Modeling for Atmospheric Science and Geophysical Fluid Dynamic, Institute of Atmospheric Physic, Chinese Academy of Sciences, Beijing 100029, China.

This article has been accepted for publication and undergone full peer review but has not been through the copyediting, typesetting, pagination and proofreading process, which may lead to differences between this version and the Version of Record. Please cite this article as doi: 10.1029/2021JD035769.

[8] State Key Laboratory of Earth Surface Processes and Resource Ecology, Beijing Normal University, Beijing 100875, China.

Corresponding author: Feng Shi (shifeng@mail.iggcas.ac.cn)

Key Points:

- The Tibetan Plateau and the Arctic experienced bidecadal cooling after two volcanic eruptions in the mid-15th century
- The heat uptake of the mid-latitude ocean caused bidecadal cooling over the Tibetan Plateau after the volcanic eruptions
- Reduced sea–air energy exchange and atmospheric poleward energy transport led to the Arctic amplification of winter temperature decrease

Abstract

Volcanic eruptions have been the most dominant natural forcing of climate change over the past millennium, affecting temperature change at multiple timescales. However, how volcanic eruptions affect regional temperature variability on the decadal timescale remains unclear. We analyzed the bidecadal effects of volcanic eruptions in the mid-15th century on two representative regions (the Tibetan Plateau (TP) and the Arctic) in the Northern Hemisphere by combining proxy reconstructions, model ensemble simulations and model sensitive experiments. The results show that the TP experienced bidecadal cooling during the mid-15th century as a result of the long-term heat uptake in the mid-latitude ocean that reduced latent heat transfer to the atmosphere. A positive sea ice–albedo feedback led to a bidecadal summer temperature decrease in the Arctic comparable to that on the TP, whereas the Arctic winter experienced stronger bidecadal cooling caused by a reduced ocean–atmosphere energy exchange and atmospheric poleward energy transport. In addition, our results show that it took ~20 years for the temperature in these two regions to return to the level that existed before the first eruption, and this was linked to the strengthening of the Atlantic Meridional Overturning Circulation and ocean heat transport.

Plain Language Summary

Simulations and reconstructions covering the past millennia show that a period of prolonged cooling developed during the mid-15th century, and this was related to the volcanic eruptions in the 1450s. We analyzed the influence of the two volcanic eruptions on Tibetan Plateau (TP) and Arctic temperatures through model-data comparison. Our results show that the inertia of the mid-latitude ocean dominated the cooling of the TP, whereas the expansion of sea ice led to the cooling of the Arctic and the adjustment of the atmospheric circulation reinforced the cooling of

the Arctic winter. In addition, the ensemble simulations indicate that the response of the Atlantic Meridional Overturning Circulation may have ended the period of cooling caused by the volcanic eruptions in the mid-15th century. This suggests that volcanic eruptions are an important factor that should be considered in the decadal prediction of regional climate and in geoengineering, especially in representative areas such as the TP and Arctic.

1 Introduction

Volcanic eruptions have been the most important natural forcing factor of climate change over the past millennium (PAGES2k Consortium, 2019). The volcanic aerosols can lead to global surface cooling and stratospheric warming via the blocking and absorption of solar radiation (Robock, 2000), and a large proportion of previous studies have focused on the interannual impact of large volcanic eruptions associated with short-lived sulfate aerosols (Adams et al., 2003; Dee et al., 2020; Robock & Mao, 1992; Stenchikov et al., 2002; Zhou et al., 2019; Zhou, 2021). Meanwhile, there is considerable evidence that volcanic eruptions may have significant effects on decadal global climate change (Church et al., 2005; Schneider et al., 2009; Slawinska & Robock, 2018). An improved understanding of the decadal volcanic impact on regional climate would be beneficial in assessing past climate variability and predicting temperature changes on the decadal scale (Bronnimann et al., 2019). However, the long-term impact of the 1991 CE Mount Pinatubo event as the only large eruption during the instrumental period on the global mean surface temperature (GMST) and regional climate is undetectable (Hansen et al., 1992, 1996; Wang et al., 2021) on account of the moderate eruptive intensity (the 16th largest volcanic eruption over the past millennia, Sigl et al., 2015).

Reginal climate change in the Tibetan Plateau (TP) and Arctic is a focus of Earth system research because of the high sensitivity of the climate in these regions to external forcings and their potential impact on the global climate. Arctic amplification (AA) has been a focus of climate research in the context of anthropogenic global warming (Serreze & Barry, 2011). Like the high climate sensitivity in the Arctic, the current warming rate of temperature in TP also is faster than the hemispherical average (Duan & Xiao, 2015; Liu & Chen, 2000; Pepin et al., 2015; Su et al. 2017). Whether there are a similar AA and a cooling in the TP over the decadal scale under the most important natural volcanic forcing is also worth exploring.

The long-term regional effects of volcanic eruptions may be linked to variations in the ocean heat content (OHC; Bronnimann et al., 2019; Church et al., 2005; Gupta & Marshall, 2018), the expansion of sea ice (Liu et al., 2020; Schneider et al., 2009; Zhong et al., 2010), and adjustments to the Atlantic Meridional Overturning Circulation (AMOC; Miller et al., 2012; Pausata et al., 2015; Slawinska & Robock, 2018; Swingedouw et al., 2015). Many studies forcus on the interannual temperature change over the TP after the eruptions, and is mainly linked to the blocking of solar radiation and the response of the El Niño-Southern Oscillation (Duan et al., 2018, 2019; Sun et al., 2019; Wang et al., 2021). There has been little focus on the decadal impacts of volcanic eruptions over the TP, and it is still unclear whether a certain ocean region dominates the decadal long-term cooling over the TP.

Some studies have suggested that volcanic eruptions have a significant impact on decadal climate variability in the Arctic (Schneider et al., 2009; Liu et al. 2020). Under the influence of four decadally paced volcanic eruptions in the second half of the 13th century, the decadal-scale expansion of sea ice after these volcanic eruptions and the related effects of the albedo feedback are thought to have been responsible for this long-term strong winter cooling in the Arctic (Schneider et al., 2009). Recently, Liu et al. (2020) showed that after the 1258 CE Samalas eruption (the strongest volcanic eruption of the past two millennia), the sea ice–albedo positive feedback and the reduction in ocean–atmosphere heat exchange may have led to strong cooling in the Arctic. Nevertheless, volcanic forcing in the last millennium has barely produced AA of a magnitude comparable with that resulting from anthropogenic greenhouse gases (GHGs; Liu et al., 2018). Moreover, as an essential component of the heat conveyer to the Arctic, a weakened AMOC in response to the volcanic eruptions would favor the sustained cooling in the Arctic (Zhong et al., 2010). After the volcanic eruptions, the expansion and transport of Arctic sea ice to the northern Atlantic Ocean can desalinate and insulate the surface waters, which can in turn suppress deep convection in the northern Atlantic Ocean and weaken the sinking branch of the AMOC (Zhong et al., 2010). The coupling between the AMOC and sea ice could lead to long-term cooling of the Arctic after volcanic eruptions, especially after multiple decadally paced volcanic eruptions (Miller et al., 2012; Zhong et al., 2010). However, some studies indicate that the AMOC would strengthen rather than weaken after volcanic eruptions (Pausata et al., 2015; Slawinska & Robock, 2018; Swingedouw et al., 2015), which leaves much uncertainty regarding the impact of volcanic eruptions on decadal climate variability in the Arctic. In general, the impacts of volcanic eruptions on decadal climate variability on the TP and in the Arctic, as well as the associated mechanisms, are yet to be fully understood.

The data–model mismatch make it difficult to analyze the response of long-term regional climate variability to volcanic eruptions. The distinct mismatch between model simulations and proxy data reconstructions should be related to the uncertainties related to internal climate variability, climatic forcing and the models themselves (Hawkins & Sutton, 2009), climate proxy data (Mann et al., 2012; Zhu et al., 2020), and proxy reconstruction methodologies (Christiansen & Ljungqvist, 2017). Nevertheless, the distinct consistency in the mid-15th century between the recent reconstructed GMST and the Coupled Model Intercomparison Project Phase 5 (CMIP5) model simulations (Fig. 2 in PAGES2k Consortium, 2019), which is also detected through a comparison between these reconstructions and the Community Earth System Model Last Millennium Ensemble (CESM–LME) simulation (Figure S1). This matching period provides an opportunity to study the effects of volcanic eruptions on regional climate under a very small anthropogenic forcing on the decadal timescale. Here, we attempt to clarify the temperature responses and the associated physical mechanisms on the TP (27°–37°N, 75°–105°E) and in the Arctic (60°–90°N) to two large volcanic eruptions in the 1450s using the CESM–LME simulation. The definition of the scopes of these two study areas is consistent with the previous studies (Liu et al. 2020; Su et al. 2017). In section 2, we introduce the ensemble simulations and reconstruction data. Section 3 presents the results. A discussion follows in section 4, and conclusions are provided in section 5.

2 Data and methods

2.1 Ensemble simulations

We used the available large ensemble of last millennium simulations from a single model, CESM–LME. The CESM–LME simulation employs version 1.1 of the CESM developed by the National Center for Atmospheric Research (NCAR). The model has approximate resolutions of 2° for the land and atmosphere components and 1° for the ocean and sea ice components (Otto-Bliesner et al., 2016). The CESM–LME contains the full-forcing simulations from 13 members forced by all forcings (solar variability, volcanic eruptions, land use, GHGs, and orbital changes) and ensembles of simulations with each forcing applied individually. The single-forcing ensemble forced by volcanic eruptions (referred to as the volcanic-only simulations) includes five members and uses the original version of the Gao et al. (2008) icecore-derived volcanic reconstruction. Using volcanic sulfate deposition from 54 Arctic and Antarctic ice cores, Gao et al. (2008) reconstructed the volcanic aerosol loading as a function of latitude, altitude, and month. In the CESM–LME, the volcanic aerosols are distributed in the bottom three layers of the stratosphere and are designated as a single-size distribution. The zonal aerosols distributed uniformly at same altitude. Because of the absence of the atmosphere component output of the first full-forcing member before 1700 CE, 12 full-forcing members were used in this work.

According to the volcanic reconstruction, two volcanic eruptions took place in the 1450s, namely the 1452 CE tropical volcanic eruption (the second-largest event of the past millennium) and the 1459 CE northern volcanic eruption (same scale as the 1963 CE Agung volcanic eruption). To analyze the impact of these two volcanic events on decadal temperatures over the TP and the Arctic, we defined the 20-year period from 1432 CE to 1451 CE as the climatological period without volcanic eruptions, and the 20-year period between 1451 CE and 1470 CE as the volcanic period. To assess the volcanic impact, we calculated the annual temperature anomalies and mean multi-year temperature anomalies (MMTA) in the volcanic period with respect to the climatological period.

2.2 Reconstruction data

We used the PAGES2k Common Era Surface Temperature Reconstructions (PAGES2k-Consortium, 2019; RT below) and Global Common Era Multiproxy Temperature Field Reconstructions (Neukom et al., 2019; RF below) datasets, both of which are based on the PAGES2k Global 2000 Year Multiproxy Database (PAGES2k-Consortium, 2017). The RT is a 2000-year annual average (April–March) GMST reconstruction ensemble generated using seven different statistical methods, and we used the ensemble median to avoid any bias from the reconstruction methods. The RF are annual mean surface temperature field reconstructions for the past two millennia, driven by six different ensemble field reconstruction methodologies. To ensure that the proxy reconstruction field was independent of the simulation field in the models, we selected the data from the reconstruction field using methods independent from the models; i.e., the canonical correlation analysis (CCA), composite plus scale (CPS), and principal component regression (PCR) approaches. In brief, these reconstruction methods establish the relationship between the instrumental temperature and the proxy records and use this relationship to obtain the temperature change before the instrumental period (see the method introduced in the above references for the specific processes).

2.3 Methods

Large ensemble is a useful method of isolating internal variability and extracting external forcing responses. In this study, we used the CESM–LME full-forcing ensemble mean to explore the climatic impact of volcanic eruptions in the mid-15th century. To exclude the interannual variability, we used a 9-year Lanczos low-pass filter (Duchon, 1979) to filter out high-frequency temperature variability. To further analyze the mechanisms associated with the strong winter cooling in the Arctic, we selected the full-forcing members whose MMTA was more negative than the ensemble average and calculated the ensemble mean of these selected members, which we refer to as the S6 ensemble. The AMOC index is defined as the maximum of the zonally averaged overturning stream function in the North Atlantic between 30°N and 60°N and between depths of 500 and 2000 m.

The upper OHC (0–700 m) is calculated as follows:

$$OHC = \int_0^{700m} Cp * \rho * T \; dZ \quad (1)$$

where Cp is the heat capacity of sea water at constant pressure; ρ is the sea water density; and T is the potential temperature.

The net sea surface energy budget (NSF) is:

$$NSF = SW + LW + SH + LH \quad (2)$$

The downward flux is uniformly defined as positive. SW and LW are the sea surface net solar radiation flux and net longwave radiation flux, respectively. SH and LH are the sea surface sensible heat flux and latent heat flux, respectively.

The vertically integrated poleward atmospheric heat transport (AHT) is calculated using the meridional internal energy, the meridional latent heat transport, and the meridional potential energy transport:

$$AHT = \int_0^{Ps} (Cp * T + Lv * Q + g * Z) * V \, dP \quad (3)$$

where Cp is the heat capacity of dry air at constant pressure; T is the air temperature; Lv is the latent heat of vaporization of water; Q is the specific humidity; Ps is the surface pressure; g is the gravitational acceleration; Z is the altitude; and V is the northward wind velocity. We have omitted the kinetic energy from this budget because it is a small component of the total energy content.

To study the role of ocean cooling in long-term climate variability over the two regions, we used a state-of-the-art model, CESM2, to conduct a sensitivity experiment (EXP_{OHC}). The horizontal resolution of the atmosphere component is 0.9° in latitude by 1.25° in longitude. We added the monthly climatological sea surface temperature (SST) anomaly of the volcanic period calculated using CESM–LME to the control experiment with the prescribed pre-industrial SST.

The experiments were run for 60 years and analyzed over the last 55 years. By analyzing the differences between EXP_{OHC} and the control experiment, we could study the separate climatic impact of the ocean cooling after the 1450s volcanic eruptions.

3 Results

3.1 Decadal temperature changes over the TP and Arctic

Figure 1 shows the simulated decadal summer (June–August, JJA) and winter (December–February, DJF) temperature anomalies for the TP and the Arctic in the CESM–LME. The simulated temperature anomalies were smoothed using a 9-year running mean to exclude interannual variability. In summer, the ensemble mean (the mean of the full-forcing ensemble) temperature changes on the TP and in the Arctic are reasonably consistent in trend and amplitude during the volcanic period, reaching a peak cooling of about −0.5℃ (Figure 1a). Unlike the summer temperature, the Arctic decadal winter temperature anomalies are significantly cooler than the TP through much of the volcanic period and are close to −1℃ when the impact was strongest (Figure 1b). The summer ensemble mean MMTA for the TP is approximately equal to that of the Arctic; i.e., about −0.26℃ during the volcanic period (Figure 1c; Table S1). In addition, the bidecadal summer cooling in the full-forcing simulations over the TP and the Arctic is comparable with the temperature change in the volcanic-only simulations in Figure 1c, and our further analysis confirmed the small influence of solar variability (Text S1). This suggests that volcanic forcing may dominate the bidecadal cooling over the TP and the Arctic.

The winter ensemble mean MMTA of the TP has a similar magnitude to its summer value, although there is a wider spread in the ensemble distribution (Figure 1c). Note that the winter ensemble mean MMTA suggests that the Arctic experienced particularly intense winter cooling (about −0.47℃) during the volcanic period (Figure 1c; Table S1), which indicates a possible AA of winter temperature decrease induced by volcanic eruptions. There are differences in the winter MMTA between the full-forcing simulations (Figure 1c, black dots) and the volcanic-only simulations (Figure 1c, green crosses), which may be related to the internal variability of the regional winter temperature.

According to the ensemble mean MMTA field in the volcanic period (Figure 2), there is a uniform cooling in summer temperature anomalies throughout the Northern Hemisphere, except for slightly stronger cooling over the Arctic, the TP, and some regions at the same latitude as the TP (Figure 2b). Especially, Arctic winter cooling amplitudes exceed those of the rest of the Northern Hemisphere, and the cooling signals are consistent among most of the ensemble members during the volcanic period (Figure 2b). Moreover, the annual mean temperature decline in the Arctic is stronger than in other parts of the Northern Hemisphere (Figure 2c) as a result of the potential winter AA (Figure 2a). The stronger winter cooling over the Arctic is also recreated by the CMIP5/PMIP3 (Taylor et al., 2012) models during the mid-15th century (Figure S2). The TP, along with the mid-latitudes, also undergoes moderately stronger cooling than the low-latitude regions, and this result is also supported by the reconstructions (Figure 2d–f) and our sensitivity experiments (Text S2; Table S2).

The anomalous solar flux caused by a single volcanic eruption in the 1450s would last only about 2 years, while volcanic aerosols have little direct influence on the winter temperature in the Arctic because of the weak insolation during the polar night (Figure S3). In contrast to the rapid and transient response of the atmosphere, some physical mechanisms discussed below could be responsible for the long-term cooling over the TP and the Arctic, leading to potential AA of the bidecadal winter temperature decline during the volcanic period.

3.2 Ocean heat content (OHC)

As the OHC simulations shown in Figure 3, short-term reductions in solar radiation caused by the volcanic eruptions in the 1450s result in a rapid decline in the heat content of the global upper oceans (upper 0–700 m), and the anomalous OHC recovers steadily after the disappearance of the direct solar radiation anomaly caused by the volcanic eruptions (Figure 3b, orange line). The continuous latent heat flux anomalies indicate that the reduced heat exchange (Figure 3b, green line) between the ocean and the lower atmosphere by evaporation is the primary way to restore OHC, cooling the global surface air temperature for an extended period.

The OHC anomaly field (Figure 3a) shows that the mid-latitude ocean (about 30°–50°N) in the Northern Hemisphere is the key area of heat content change. Consequently, during ocean heat restoration (Figure 3b, orange line), the cooling effect on the mid-latitude atmosphere through latent heat exchange is also more severe than at other latitudes (Figure 3b, green dashed line). This restoration of the mid-latitude OHC caused the bidecadal cooling of the TP during the volcanic period, which was slightly more robust than that of the continental regions at low latitudes (Text S2). According to the changes in the mid-latitude sea surface energy budget in winter and summer (not shown), it can be found that the latent heat exchange anomalies of the two seasons lasted until the end of the 1460s. Our atmospheric sensitivity experiment also shows that the long-term cooling of the ocean can lead to a cooling of ~0.21℃ over the TP (Table S1). Considering the direct cooling caused by the volcanic aerosols in the full-forcing simulations, the magnitude of temperature decrease is consistent with the results from CESM–LME (~0.29℃, Table S1), which reveals the inertia of the OHC dominated the bidecadal cooling of the TP.

However, there is no significant difference in Arctic summer ocean–atmosphere heat exchange between the volcanic period and the climatological period, which shows that the local recovery of the OHC does not contribute to the long-term summer temperature anomaly in the Arctic (Figure 4a). The summer net energy flux in Figure 4a fluctuates significantly before 1462 CE, which is related to the net solar radiation (Figure 4a, red line) rather than the OHC. The result of winter ocean–atmosphere heat exchange in the Arctic shows significant negative anomalies (i.e., positive anomalies in Figure 4b, implying increased downward flux from atmosphere to the ocean) in the sensible heat flux and longwave flux from the ocean to the atmosphere several years after the 1452 CE volcanic eruption (Figure 4b, purple and blue lines). This obviously differs to the interpretation of the OHC that the global ocean–atmosphere heat exchange anomaly was dominated mainly by the latent heat flux during most of the volcanic period (Figure 3b, green line). This may indicate that the change of winter ocean–atmosphere heat exchange in the Arctic is not influenced by the restoration of the OHC.

3.3 Sea ice

The anomalous expansion of Arctic sea ice (of about 2% with respect to the climatological mean extent) persists for over 10 years, and the winter area anomaly of sea ice is slightly, but non-significantly, larger than the summer area anomaly throughout most of the volcanic period (Figure 5). Even after the volcanic aerosol deposition, the net solar radiation anomaly of the Arctic surface remains negative for an extended period (Figure 4a), which leads to the long-term summer cooling of the Arctic since the expansion of sea ice increases the surface albedo of the Arctic. It is worth noting that the Arctic summer temperature recovery is about 3 years later than the net solar radiation, which may be related to the inertia of the Arctic Ocean.

The sea ice–albedo feedback has little direct impact on winter surface radiation (Figure S3), since most of the Arctic is in the polar night during the winter. The short-term summer solar radiation decline caused by volcanic eruptions and the sea ice–albedo feedback trigger and maintain the expansion of the sea ice. The increased extent of the sea ice blocks the energy exchange (including latent heat, sensible heat, and longwave radiation) between the ocean and the atmosphere in winter, indicating that the expansion of the sea ice remains the dominant cause of the bidecadal winter cooling of the Arctic (Figure 4b).

Note that heat exchange between the ocean and the atmosphere increases significantly in the 1452/1453 CE winter over the Arctic. After the volcanic eruptions, the strengthened AMOC conveys more heat to the mid- and high-latitude Arctic Ocean from low latitudes (Figure 6). Moreover, the extent of the sea ice has not yet increased significantly in the first winter following the 1452 CE volcanic event, which leads to more heat transfer in this winter from the Arctic Ocean to the atmosphere. The stronger AMOC also provokes the significant intensification of ocean–atmosphere energy exchange in the winter of 1450 CE. Subsequently, with the expansion of the sea ice, the shrinking of the area of open water limits the ability of the lower atmosphere to gain heat from the ocean, inducing continuous cooling during the Arctic winter.

With the winter sea ice anomaly gradually recovering around 1464 CE, the energy exchange anomaly no longer dominates the Arctic winter cooling (Figure 4). However, despite the disabled energy exchange anomaly in the first few years after the 1452 CE volcanic event and late 1460s, the Arctic winter temperature decline persists for ~20 years, which implies that factors other than the reduced energy exchange may reinforce the robust bidecadal winter cooling in the Arctic.

3.4 Atmospheric circulation

During the winters of the volcanic period, there are significant negative 200-hPa geopotential height anomalies in the high latitudes of the Northern Hemisphere (Figure 7). We selected the six members of the full-forcing ensemble simulations (S6) with stronger bidecadal winter cooling in the Arctic to analyze the atmospheric circulation associated with the winter cooling. The model simulated a moderate increase or no change in geopotential height in the mid-latitudes, especially around the Aleutian Islands and the eastern United States, which contributed to the negative phase of the Pacific/North American teleconnection pattern (nPNA; Figure 7a). The response of the geopotential height in the S6 ensemble (Figure 7b) is more significant than that of the full-forcing ensemble (Figure 7a), and the anomalous wind field is also more evident, resulting in stronger winter cooling in the Arctic.

We also analyzed the bidecadal change in geopotential height and wind during similar periods influenced by volcanic eruptions (i.e., the mid-13th and early 19th centuries). The results show that an nPNA-like response also occurred following these other eruptions (Figures S4 and S5). The positive geopotential anomalies and anticyclones located in the middle of the North Pacific span the entire troposphere, especially in members with the stronger winter cooling. An anomalous AHT is simulated in the North Pacific (60°N, 150°E–150°W), a region that exhibits a significant atmospheric circulation response and is crucial to the atmospheric heat engine. The results show that the decrease of AHT continued for ~20 years after the first volcanic eruptions, especially in S6 (Figure S6). The anomalous anticyclones intensify the westerly wind around the Arctic Ocean, confining the cold air to the Arctic Ocean and blocking the transport of heat and water vapor from the North Pacific to the Arctic Ocean, which is another important cause of the strong bidecadal winter cooling in the Arctic.

3.5 Ocean circulation

The AMOC strength increased significantly in the 30 years following the volcanic eruption in 1452 CE (Figure 6a), and the surface salinity of the Northern Atlantic Ocean was anomalously high during the volcanic period (Figure 8a). As a consequence of the increased surface salinity, the density of the upper ocean increased significantly, which is crucial to the stability of the water column and the intensity of oceanic convection, resulting in the decadally strengthened AMOC during the volcanic period. The salinity continuously increased in the Labrador Sea (Figure 8b), even when the sea ice and AMOC anomalies faded during the period 1471–1490 CE (Figure 6a). In contrast, the salinity in the subpolar North Atlantic (50°–60°N, 20°–50°W) increased during the volcanic period (Figure 8a) and then recovered following the change in sea ice extent (Figure 8b). These results indicate a prolonged reduction in the barotropic stream function in the subpolar North Atlantic rather than the Labrador Sea during the volcanic period (Figure 8c), which corresponds to a strengthening of the AMOC. Subsequently, the increased barotropic stream function suggests that deep convection is suppressed in the subpolar North Atlantic, favoring the deceleration of the AMOC after the volcanic period (Figure 8d).

4 Discussion

In the CESM–LME, there are similar long-term cooling events over the TP and the Arctic over the periods 1257–1276 CE and 1808–1827 CE (Figure S7). The Samalas volcanic eruption in Indonesia—the largest volcanic eruption of the past millennium (Guillet et al., 2017)—and two southern volcanic eruptions occurred between 1257 and 1276 CE. Two tropical volcanic events, including the 1815 CE Tambora eruption, took place between 1808 and 1827 CE. Although the volcanic eruptions during these two periods and in the mid-15th century occurred at different latitudes, there are consistent changes in summer temperature between the TP and the Arctic, with comparable bidecadal winter temperature decreases on the TP and the potential AA of the bidecadal winter temperature decline under the volcanic impacts. The composite temperature anomalies for these two periods and the mid-15th century show that the comparisons between the TP and Arctic are also supported by interannual temperature responses (Figure S8).

Furthermore, the winter temperature decline over the Arctic is weaker than on the TP before the stronger 1815 CE Tambora eruption during the early 19th century (Figure S7e). In the other two periods (mid-13th and mid-15th centuries), larger volcanic eruptions occurred before moderate volcanic eruptions, which implies that only exceptionally strong volcanic eruptions can trigger AA. This result may explain the undetectable AA when considering the volcanic forcing over the past millennium (Liu et al., 2018).

Although accompanied by potential hydrological impacts, the long-term cooling caused by volcanic eruptions may act as a significant natural geoengineering effect that can counteract anthropogenic warming (Crutzen, 2006; Robock et al., 2008). Compared with the GHG-only simulations, the bidecadal cooling induced by the 1450s volcanic eruptions could have offset ~25% (16%) of the GHG-induced warming over the TP (Arctic) over the last century (Table S1). This suggests that volcanic eruptions are an important factor that should be incorporated into decadal-scale predictions of regional climate and any geoengineering-based mitigation strategies.

The long-term response of the OHC is a critical part of the physical mechanism of the ongoing climate impact of volcanic eruptions (Bronnimann et al., 2019; Ding et al., 2014; Stenchikov et al., 2009). However, it remains unclear how the volcanic eruptions cool a given region via the associated OHC processes. The pattern of the ensemble mean MMTA field is consistent with proxy reconstructions of the Northern Hemisphere during the volcanic period, indicating that the mid-latitude region experienced stronger bidecadal cooling than the tropics. The model results further show that heat content and heat uptake (latent heat exchange) anomalies in the mid-latitude oceans were more significant than those in other latitudes. In addition, under the influence of two tropical volcanic eruptions in the early 19th century, there was also a stronger mid-latitude cooling, where again the ocean heat uptake at mid-latitudes was stronger than at other latitudes (Figure S9, green dashed line), implying that the restoration of the mid-latitude OHC was the key cause of bidecadal cooling over the TP. The reconstructed and simulated temperature time series are consistent with the MMTA patterns and support the stronger heat uptake process in the mid-latitude ocean (Figure S10).

The Rossby wave train may play an important role in connecting the long-term heat uptake of mid-latitude oceans and bidecadal cooling over the TP. Our sensitivity experiment shows that there are anomalous atmospheric wave trains at the top of the troposphere in summer in the Northern Hemisphere (Figure S11), which may be an essential process linking the ocean and mid-latitude land cooling. Previous studies have found that sea surface temperatures in the North Atlantic can influence mid-latitude temperatures during the winter via a wave train (Sun et al., 2016), although there is no significant evidence for an anomalous wave train in the ensemble mean simulation. This absence may be related to the large internal variability of the atmosphere and the differing response of the Rossby wave among ensemble members.

The sea ice–albedo feedback is generally considered to be the direct cause of the long-term cooling of the Arctic under the influence of volcanic eruptions (Schneider et al., 2009), and our results indicate that the increased reflected solar radiation caused by the expansion of the sea ice resulted in the long-term summer cooling in the Arctic during the mid-15th century. During the climatological winter, due to the rapid cooling of the lower troposphere, the energy exchange between the ocean and the atmosphere is a vital factor in maintaining the Arctic surface air temperature (Serreze et al., 2007). Hence, the reduced ocean–atmosphere energy exchange induced by expanded sea ice coverage contributes to the winter temperature decrease of the Arctic on the decadal timescale. Our result is consistent with the sensitivity experiments related to the Samalas volcanic eruption (Liu et al., 2020) and is the opposite mechanism to that associated with the newly opened waters and stronger seasonal energy exchange under global warming (Dai et al., 2019; Serreze et al., 2007).

Previous studies focused on the direct impact of sulfate aerosols generated by a single volcanic event on the atmospheric circulation (Robock, 2000; Zambri & Robock, 2016), but there was little discussion of the impact of the adjusted atmospheric circulation on the decadal climate in the Arctic after successive eruptions. A previous study pointed out that volcanic eruptions observed during the instrumental period have triggered a positive phase of the PNA pattern during the subsequent winter (Liu et al., 2016). However, it remains unclear how the PNA pattern responds to volcanic eruptions at the decadal scale, and especially how it responded to explosive volcanic eruptions that occurred prior to the instrumental period. Our results show that the nPNA-like response during the mid-15th century combined with the reduced energy exchange to strongly cool the Arctic winter. The relationship between the response of the atmospheric circulation and the stronger Arctic winter cooling during the mid-15th century can be detected in other climate models. The simulation over the last millennium using the GISS-E2-R model (member 122; Schmidt et al., 2006) shows similar results that the strongest decadal winter cooling on the eastern flank of the anomalous anticyclones (i.e., North America and Eastern Europe; Figure S12), which is forced by the same volcanic forcing but different solar forcing to the CESM–LME simulations.

Our results show that the decrease in AHT continued for ~20 years, especially in the S6 ensemble (Figure S6), which led to a strong winter cooling in the Arctic and thicker and wider sea ice in the Chukchi and Bering seas (Figure S13). This indicates that the climatic effect of the nPNA-like response may be exactly the opposite of the positive PNA pattern, leading to the stronger winter cooling in the Arctic during the mid-15th century since the positive PNA pattern is verified to lead to increased heat and moisture fluxes into the Arctic from the advection of North Pacific airmasses (Liu et al., 2021). In addition, the Aleutian Low, as an essential component of the PNA, has been shown to have a dominant effect on the winter temperature in the Arctic Pacific region, even over centennial scales (Rodionov et al., 2005; Zhong et al., 2018).

Under the impact of two large volcanic eruptions in the mid-15th century (one of the eruptions was the second-largest of the past millennium), the TP and the Arctic, two of the regions that are most sensitive to external forcing, experienced cooling for no longer than 20 years. Although the recovery of the OHC lasted for several decades, the heat uptake related to latent heat exchange increased significantly for only ~20 years after the first volcanic eruption, which may have led to the recovery of the temperature over the TP to pre-eruption levels at the end of the volcanic period. The increased extent of the sea ice reflects summer solar radiation and impedes winter heat transport from the ocean to the atmosphere, leading to the Arctic cooling on the decadal timescale. Our results show that the anomalous sea-ice extent and the nPNA-like atmospheric circulation may be the key causes of the bidecadal cooling in the Arctic. The expansion of the Arctic sea ice lasted only a little more than 10 years, so the Arctic temperature recovered to the pre-eruption level at the end of the volcanic period.

The temperature recovery and the interruption of the potential initiation of the Little Ice Age may be related to increased oceanic northward heat transport by the stronger AMOC in the second half of the 15th century. The strengthened AMOC led to increased oceanic northward heat transport after the two decadally paced large volcanic eruptions in the ensemble simulations (Figure 6b), contributing to the recovery of the sea ice and mid-latitude ocean, which results in the simulated bidecadal temperature decrease instead of decades, or even a century of colder temperature.

Some studies have suggested that decreased precipitation and river runoff at high latitudes of the Northern Hemisphere, and the reduced input of fresh water from the Arctic Ocean, contributed to the salinization in the northern Atlantic after volcanic eruptions, especially in the Labrador Sea where convective activity plays a crucial role in the deep water formation associated with the AMOC (Slawinska & Robock, 2018; Stenchikov et al., 2009; Swingedouw et al., 2015; Zhong et al., 2010). Instead, our results show that the deep convection in the subpolar North Atlantic dominated the variability of the AMOC after the volcanic eruptions during the latter half of the 15th century. Our result is consistent with to a robust observation (Chafik & Rossby, 2019; Lozier et al., 2019) that the oceanic convection in the subpolar region and the Nordic seas is more likely to be responsible for the variability of the AMOC than convection in the Labrador Sea, as is traditionally believed. The correspondence between decadal variability of the subpolar deep convection and the evolution of the AMOC reveals the crucial role played by the subpolar North Atlantic, rather than the Labrador Sea, in decadal climate fluctuations during the mid-15th century.

5 Conclusions

Our aim for this study was to use the CESM–LME simulations, atmospheric sensitive experiment, and proxy temperature reconstructions to improve our understanding of the influence of the volcanic eruptions in the mid-15th century on decadal temperature variability over the TP and the Arctic. Our major findings are summarized below.

1) Following two large volcanic eruptions, the TP and Arctic experienced bidecadal cooling in the mid-15th century. The bidecadal cooling (~0.26℃ over the period 1451–1470 CE) of the Arctic summer was similar to the cooling of the summer and winter on the TP, which was moderately stronger than the tropical cooling. In contrast, the Arctic winter temperature showed a marked bidecadal decline (~0.47℃).
2) The bidecadal cooling over the summer and winter TP may be linked to the increased oceanic heat uptake in mid-latitudes via a Rossby wave. The sea ice–albedo positive feedback caused the bidecadal decrease in the Arctic summer temperature. Moreover, the reduced ocean–atmosphere energy exchange related to the expansion of the sea ice and the reduced atmospheric poleward energy transport coupled with the nPNA-like atmospheric circulation caused the significant bidecadal cooling of the Arctic winter.
3) After the two explosive volcanic eruptions on the temperatures in these two regions, the temperatures recovered after two decades in response to the increased strength of the AMOC and associated northward ocean heat transport.

Although the TP and the Arctic are both sensitive to external forcing, and their cooling under the influence of volcanic eruptions is stronger than that in low-latitude regions, our results show that the mechanisms associated with bidecadal cooling in the two regions during the mid-15th century were distinctly different. The potential response of the mid-latitude ocean and Arctic sea ice to the AMOC may imply an indirect connection between the TP and the Arctic, and this may explain why the temperature in both regions returned to pre-eruption levels ~20 years after the first volcanic eruption. Therefore, the internal variability, such as PNA and AMOC, may play essential roles in long-term regional temperature variability after volcanic eruptions.

Acknowledgments

This work was jointly funded by the National Natural Science Foundation of China (Grant Nos. 41888101; 42077406; 41877440), the Strategic Priority Research Program of Chinese Academy of Sciences (Grant No. XDB26020204), and the Key Research Program of the Institute of Geology & Geophysics, CAS (Grant No. IGGCAS-201905). Feng Shi is funded by the Youth Innovation Promotion Association CAS. Qiuzhen Yin is Research Associate of F.R.S-FNRS (Belgium).

Author contributions

F.S. and Z.T.G. coordinated the project and designed the study. W.L. analyzed model and reconstruction results. W.L., F.S., H.H.X., and F.L. contributed to mechanism analysis. W.L. made the figures. W.L. and F.S. wrote the paper. W.L., F.S., G.Q.X., H.H.X., Q.Z.Y., F.L., A.M.D., C.D.X. and Z.T.G. discussed the results and contributed to the writing.

Competing interests

The authors declare no competing financial interests.

Data and materials availability

The CESM-LME dataset is available at: https://www.earthsystemgrid.org/dataset/ucar.cgd.ccsm4.cesmLME.html. PAGES2k Common

Era Surface Temperature Reconstructions was archived in the NOAA data repository (https://www.ncdc.noaa.gov/paleo-search/study/26872). Global Common Era Multiproxy Temperature Field Reconstructions was archived in the NOAA data repository (https://www.ncdc.noaa.gov/paleo-search/study/26850).

References

Adams, J. B., Mann, M. E., & Ammann, C. M. (2003). Proxy evidence for an El Nino-like response to volcanic forcing. *Nature, 426*(6964), 274–278. https://doi.org/10.1038/nature02101

Bronnimann, S., Franke, J., Nussbaumer, S. U., Zumbuhl, H. J., Steiner, D., Trachsel, M., et al. (2019). Last phase of the Little Ice Age forced by volcanic eruptions. *Nature Geoscience, 12*(8), 650–656. https://doi.org/10.1038/s41561-019-0402-y

Chafik, L., & Rossby, T. (2019). Volume, heat, and freshwater divergences in the subpolar North Atlantic suggest the Nordic Seas as key to the state of the meridional overturning circulation. *Geophysical Research Letters, 46*(9), 4799–4808. https://doi.org/10.1029/2019gl082110

Christiansen, B., & Ljungqvist, F. C. (2017). Challenges and perspectives for large-scale temperature reconstructions of the past two millennia. *Reviews of geophysics, 55*(1), 40–96. https://doi.org/10.1002/2016rg000521

Church, J. A., White, N. J., & Arblaster, J. M. (2005). Significant decadal-scale impact of volcanic eruptions on sea level and ocean heat content. *Nature, 438*(7064), 74–77. https://doi.org/10.1038/nature04237

Crutzen, P. J. (2006). Albedo enhancement by stratospheric sulfur injections: A contribution to eesolve a policy dilemma? *Climatic Change, 77*(3–4), 211–220. https://doi.org/10.1007/s10584-006-9101-y

Dai, A., Luo, D., Song, M., & Liu, J. (2019). Arctic amplification is caused by sea-ice loss under increasing CO2. *Nature Communications, 10*(1), 121. https://doi.org/10.1038/s41467-018-07954-9

Dee, S. G., Cobb, K. M., Emile-Geay, J., Ault, T. R., Edwards, R. L., Cheng, H., & Charles, C. D. (2020). No consistent ENSO response to volcanic forcing over the last millennium. *Science, 367*(6485), 1477. https://doi.org/10.1126/science.aax2000

Ding, Y., Carton, J. A., Chepurin, G. A., Stenchikov, G., Robock, A., Sentman, L. T., & Krasting, J. P. (2014). Ocean response to volcanic eruptions in Coupled Model Intercomparison Project 5 simulations. *Journal of Geophysical Research: Oceans, 119*(9), 5622–5637. https://doi.org/10.1002/2013jc009780

Duan, A., & Xiao, Z. (2015). Does the climate warming hiatus exist over the Tibetan Plateau? *Scientific Reports, 5*, 13711. https://doi.org/10.1038/srep13711

Duan, J., Li, L., Ma, Z., Esper, J., Büntgen, U., Xoplaki, E., et al. (2018). Summer cooling driven by large volcanic eruptions over the Tibetan Plateau. *Journal of Climate, 31*(24), 9869–9879. https://doi.org/10.1175/JCLI-D-17-0664.1

Duan, J., Wu, P., & Ma, Z. (2019). Reconciling the discrepancy of post-volcanic cooling estimated from tree-ring reconstructions and model simulations over the Tibetan Plateau. *Atmosphere, 10*(12). https://doi.org/10.3390/atmos10120738

Duchon, C. E. (1979). Lanczos filtering in one and two dimensions. *Journal of Applied Meteorology, 18*(8), 1016–1022. https://doi.org/10.1175/1520-0450(1979)018<1016:Lfioat>2.0.Co;2

Guillet, S., Corona, C., Stoffel, M., Khodri, M., Lavigne, F., Ortega, P., et al. (2017). Climate response to the Samalas volcanic eruption in 1257 revealed by proxy records. *Nature Geoscience, 10*(2), 123–128. https://doi.org/10.1038/ngeo2875

Gupta, M., & Marshall, J. (2018). The climate response to multiple volcanic eruptions mediated by ocean heat uptake: Damping processes and accumulation potentia. *Journal of Climate, 31*(21), 8669–8687. https://doi.org/10.1175/jcli-d-17-0703.1

Hansen, J., Lacis, A., Ruedy, R., & Sato, M. (1992). Potential climate impact of Mount Pinatubo eruption. *Geophysical Research Letters, 19*(2), 215–218. https://doi.org/10.1029/91gl02788

Hansen, J., Ruedy, R., Sato, M., & Reynolds, R. (1996). Global surface air temperature in 1995: Return to pre-Pinatubo level. *Geophysical Research Letters, 23*(13), 1665–1668. https://doi.org/10.1029/96gl01040

Hawkins, E., & Sutton, R. (2009). The potential to narrow uncertainty in regional climate predictions. *Bulletin of the American Meteorological Society, 90*(8), 1095–1108. https://doi.org/10.1175/2009bams2607.1

L'Heureux, M. L., Kumar, A., Bell, G. D., Halpert, M. S., & Higgins, R. W. (2008). Role of the Pacific-North American (PNA) pattern in the 2007 Arctic sea ice decline. *Geophysical Research Letters, 35*(20). https://doi.org/10.1029/2008gl035205

Liu, B., Wang, B., Liu, J., Chen, D., Ning, L., Yan, M., et al. (2020). Global and polar region temperature change induced by single mega volcanic eruption based on Community Earth System Model simulation . *Geophysical Research Letters, 47*(18). https://doi.org/10.1029/2020gl089416

Liu, F., Zhao, T., Wang, B., Liu, J., & Luo, W. (2018). Different global precipitation responses to solar, volcanic, and greenhouse gas forcings. *Journal of Geophysical Research: Atmospheres, 123*(8), 4060–4072. https://doi.org/10.1029/2017jd027391

Liu, X., & Chen, B. (2000). Climatic warming in the Tibetan Plateau during recent decades. *International Journal of Climatology*, *20*(14), 1729–1742. https://doi.org/10.1002/1097-0088(20001130)20:14<1729::AID-JOC556>3.0.CO;2-Y

Liu, Z., Risi, C., Codron, F., He, X., Poulsen, C. J., Wei, Z., et al. (2021). Acceleration of western Arctic sea ice loss linked to the Pacific North American pattern. *Nature Communications*, *12*(1), 1519. https://doi.org/10.1038/s41467-021-21830-z

Liu, Z., Yoshimura, K., Buenning, N. H., Jian, Z., & Zhao, L. (2016). The response of winter Pacific North American pattern to strong volcanic eruptions. *Climate Dynamics*, *48*(11–12), 3599–3614. https://doi.org/10.1007/s00382-016-3287-0

Lozier, M. S., Li, F., Bacon, S., Bahr, F., Bower, A. S., Cunningham, S. A., et al. (2019). A sea change in our view of overturning in the subpolar North Atlantic. *Science*, *363*(6426), 516–521. https://doi.org/10.1126/science.aau6592

Mann, M. E., Fuentes, J. D., & Rutherford, S. (2012). Underestimation of volcanic cooling in tree-ring-based reconstructions of hemispheric temperatures. *Nature Geoscience*, *5*(3), 202–205. https://doi.org/10.1038/ngeo1394

Mann, M. E., Steinman, B. A., Brouillette, D. J., & Miller, S. K. (2021). Multidecadal climate oscillations during the past millennium driven by volcanic forcing. *Science*, *371*(6533), 1014–1019. https://doi.org/10.1126/science.abc5810

Miller, G. H., Geirsdottir, A., Zhong, Y. F., Larsen, D. J., Otto-Bliesner, B. L., Holland, M. M., et al. (2012). Abrupt onset of the Little Ice Age triggered by volcanism and sustained by sea-ice/ocean feedbacks. *Geophysical Research Letters*, *39*(2), L02708. https://doi.org/10.1029/2011gl050168

Neukom, R., Steiger, N., Gomez-Navarro, J. J., Wang, J., & Werner, J. P. (2019). No evidence for globally coherent warm and cold periods over the preindustrial Common Era. *Nature, 571*(7766), 550–554. https://doi.org/10.1038/s41586-019-1401-2

Otto-Bliesner, B. L., Brady, E. C., Fasullo, J., Jahn, A., Landrum, L., Stevenson, S., et al. (2016). Climate variability and change since 850 CE: An ensemble approach with the Community Earth System Model. *Bulletin of the American Meteorological Society, 97*(5), 735–754. https://doi.org/10.1175/BAMS-D-14-00233.1

PAGES2k-Consortium. (2017). A global multiproxy database for temperature reconstructions of the Common Era. *Scientific data, 4*, 170088. https://doi.org/10.1038/sdata.2017.88

PAGES2k-Consortium. (2019). Consistent multidecadal variability in global temperature reconstructions and simulations over the Common Era. *Nature Geoscience*, *12*(8), 643–649. https://doi.org/10.1038/s41561-019-0400-0

Pausata, F. S., Chafik, L., Caballero, R., & Battisti, D. S. (2015). Impacts of high-latitude volcanic eruptions on ENSO and AMOC. *Proceedings of the National Academy of Sciences, 112*(45), 13784–13788. https://doi.org/10.1073/pnas.1509153112

Pepin, N., Bradley, R. S., Diaz, H. F., Baraer, M., Caceres, E. B., Forsythe, N., et al. (2015). Elevation-dependent warming in mountain regions of the world. *Nature Climate Change, 5*(5), 424–430. https://doi.org/10.1038/nclimate2563

Robock, A. (2000). Volcanic eruptions and climate. *Reviews of geophysics, 38*(2), 191–219. https://doi.org/10.1029/1998rg000054

Robock, A., & Mao, J. (1992). Winter warming from large volcanic eruptions. *Geophysical Research Letters, 19*(24), 2405–2408. https://doi.org/10.1029/92gl02627

Robock, A., Oman, L., & Stenchikov, G. L. (2008). Regional climate responses to geoengineering with tropical and Arctic SO2injections. *Journal of Geophysical Research, 113*(D16). https://doi.org/10.1029/2008jd010050

Rodionov, S. N., Overland, J. E., & Bond, N. A. (2005). The Aleutian low and winter climatic conditions in the Bering Sea. Part I: Classification. *Journal of Climate, 18*(1), 160–177. https://doi.org/10.1175/jcli3253.1

Schmidt, G. A., Ruedy, R., Hansen, J. E., Aleinov, I., Bell, N., Bauer, M., et al. (2006). Present-day atmospheric simulations using GISS ModelE: Comparison to in situ, satellite, and reanalysis data. *Journal of Climate, 19*(2), 153–192. https://doi.org/10.1175/jcli3612.1

Schneider, D. P., Ammann, C. M., Otto-Bliesner, B. L., & Kaufman, D. S. (2009). Climate response to large, high-latitude and low-latitude volcanic eruptions in the Community Climate System Model. *Journal of Geophysical Research, 114*(D15). https://doi.org/10.1029/2008jd011222

Serreze, M. C., Barrett, A. P., Slater, A. G., Steele, M., Zhang, J., & Trenberth, K. E. (2007). The large-scale energy budget of the Arctic. *Journal of Geophysical Research, 112*(D11). https://doi.org/10.1029/2006jd008230

Serreze, M. C., & Barry, R. G. (2011). Processes and impacts of Arctic amplification: A research synthesis. *Global and Planetary Change, 77*(1-2), 85–96. https://doi.org/10.1016/j.gloplacha.2011.03.004

Sigl, M., Winstrup, M., McConnell, J. R., Welten, K. C., Plunkett, G., L`udlow, F., et al. (2015). Timing and climate forcing of volcanic eruptions for the past 2,500 years. *Nature, 523*(7562), 543–549. https://doi.org/10.1038/nature14565

Slawinska, J., & Robock, A. (2018). Impact of volcanic eruptions on decadal to centennial fluctuations of Arctic sea ice extent during the last millennium and on initiation of the Little Ice Age. *Journal of Climate, 31*(6), 2145–2167. https://doi.org/10.1175/Jcli-D-16-0498.1

Stenchikov, G., Delworth, T. L., Ramaswamy, V., Stouffer, R. J., Wittenberg, A., & Zeng, F. R. (2009). Volcanic signals in oceans. *Journal of Geophysical Research:Atmospheres, 114*(D16), D16104. https://doi.org/10.1029/2008jd011673

Stenchikov, G., Robock, A., Ramaswamy, V., Schwarzkopf, M. D., Hamilton, K., & Ramachandran, S. (2002). Arctic Oscillation response to the 1991 Mount Pinatubo eruption: Effects of volcanic aerosols and ozone depletion. *Journal of Geophysical Research: Atmospheres, 107*(D24), ACL 28. https://doi.org/10.1029/2002jd002090

Su, J., Duan, A., & Xu, H. (2017). Quantitative analysis of surface warming amplification over the Tibetan Plateau after the late 1990s using surface energy balance equation. *Atmospheric Science Letters, 18*(3), 112–117. https://doi.org/10.1002/asl.732

Sun, C., Li, J., Ding, R., & Jin, Z. (2016). Cold season Africa–Asia multidecadal teleconnection pattern and its relation to the Atlantic multidecadal variability. *Climate Dynamics, 48*(11–12), 3903–3918. https://doi.org/10.1007/s00382-016-3309-y

Sun, D., Zheng, J., Zhang, X., & Hao, Z. (2019). The relationship between large volcanic eruptions in different latitudinal zones and spatial patterns of winter temperature anomalies over China. *Climate Dynamics, 53*(9–10), 6437–6452. https://doi.org/10.1007/s00382-019-04937-4

Swingedouw, D., Ortega, P., Mignot, J., Guilyardi, E., Masson-Delmotte, V., Butler, P. G., et al. (2015). Bidecadal North Atlantic ocean circulation variability controlled by timing of volcanic eruptions. *Nature Communications, 6*(1), 6545. https://doi.org/10.1038/ncomms7545

Taylor, K. E., Stouffer, R. J., & Meehl, G. A. (2012). An overview of CMIP5 and the experiment design. *Bulletin of the American Meteorological Society, 93*(4), 485–498. https://doi.org/10.1175/bams-d-11-00094.1

Wang, Y., Shao, X., Zhang, Y., & Li, M. (2021). The response of annual minimum temperature on the eastern central Tibetan Plateau to large volcanic eruptions over the period 1380–2014 CE. *Climate of the Past, 17*(1), 241–252. https://doi.org/10.5194/cp-17-241-2021

Zambri, B., & Robock, A. (2016). Winter warming and summer monsoon reduction after volcanic eruptions in Coupled Model Intercomparison Project 5 (CMIP5) simulations. *Geophysical Research Letters, 43*(20), 10,920–10,928. https://doi.org/10.1002/2016gl070460

Zhong, Y., Jahn, A., Miller, G. H., & Geirsdottir, A. (2018). Asymmetric cooling of the Atlantic and Pacific Arctic during the past two millennia: A dual observation-modeling study. *Geophysical Research Letters, 45*(22), 12,497–12,505. https://doi.org/10.1029/2018gl079447

Zhong, Y., Miller, G. H., Otto-Bliesner, B. L., Holland, M. M., Bailey, D. A., Schneider, D. P., & Geirsdottir, A. (2010). Centennial-scale climate change from decadally-paced explosive volcanism: a coupled sea ice-ocean mechanism. *Climate Dynamics, 37*(11–12), 2373–2387. https://doi.org/10.1007/s00382-010-0967-z

Zhou, T., Zuo, M., & Man, W. (2019). Hydroclimate responses over global monsoon regions following volcanic eruptions at different latitudes. *Journal of Climate, 32*(14), 4367–4385. https://doi.org/10.1175/Jcli-D-18-0707.1

Zhou, T. (2021). New physical science behind climate change: What does IPCC AR6 tell us? *The Innovation*, *2*(4), 100173. https://doi.org/10.1016/j.xinn.2021.100173

Zhu, F., Emile-Geay, J., Hakim, G. J., King, J., & Anchukaitis, K. J. (2020). Resolving the differences in the simulated and reconstructed temperature response to volcanism. *Geophysical Research Letters*, *47*(8), e2019GL086908. https://doi.org/10.1029/2019GL086908

Figure Captions

Figure 1. Simulated anomalies of TP (ensemble mean, red line) and Arctic (ensemble mean, blue line) temperatures in summer (a) and winter (b), and the regional multi-year mean temperature (c) of the volcanic period (1451–1470 CE). Temperature anomalies were smoothed with a 9-year running-mean and the shading represents the 95% ensemble spread. Boxes represent the interquartile range and whiskers represent the minimum and maximum. Black dots represent the ensemble mean of the full-forcing simulations and only green crosses indicate the ensemble mean of volcanic-only simulations. Anomalies are relative to 1432–1451 CE.

Figure 2. Temperature anomalies over the volcanic period. Ensemble mean winter (a), summer (b), and annual (c) temperature anomalies of the full-forcing ensemble. Hatching indicates where anomalies have the same sign in fewer than eight members. Methods used for the reconstructed mean annual temperature were CCA (d), PCR (e), and CPS (f). Zonal mean anomalies are shown in the right panels. The TP (27°–37°N, 75°–105°E) is outlined by the red box and the black contour denotes areas with elevations above 3,000 m.

Figure 3. Upper ocean heat content anomaly (a) and sea surface energy budget (b) during the volcanic period. Colored solid lines indicate the mean flux over the global ocean and the green dashed line indicates the mean latent heat flux over the mid-latitude ocean (30°–50°N); the sign of convention is positive downward. The orange line represents the global mean upper ocean heat content anomaly (0–700 m, units: 10^{22} J) in (b). Shading represents the 95% ensemble spread. SW = net solar radiation flux, LW = net longwave radiation flux, SH = sensible heat flux,

LH = latent heat flux, NSF = net surface energy flux, M–LH = latent heat flux over mid-latitude ocean, and OHC = upper ocean heat content.

Figure 4. Summer (a) and winter (b) anomalies in the sea surface energy budget in the Arctic during the volcanic period. Vertical gray dashed lines represent the years of the eruptions. Positive values indicate that energy is transferred downward. Shading represents the 95% ensemble spread. SW = net solar radiation flux, LW = net longwave radiation flux, SH = sensible heat flux, LH = latent heat flux, and NSF = net surface energy flux.

Figure 5. Summer (red line) and winter (blue line) sea-ice-extent anomalies in the Arctic during the volcanic period. Shading represents the 95% ensemble spread. Red bars indicate the volcanic forcing.

Figure 6. Anomalies of AMOC (a) and the North Atlantic northward heat transport (b). The AMOC index is the maximum in the zonally averaged overturning stream function in the North Atlantic between 30°N and 60°N, and between depths of 500 and 2000 m, and the heat transport is calculated using the average meridional heat transport in the North Atlantic at 60°N. Solid lines are the ensemble mean and the shading indicates the 95% ensemble spread. The correlation coefficient between the anomalous AMOC and northward heat transport is 0.60 during the period 1450–1499 CE, which is statistically significant at the level of 0.1%.

Figure 7. Winter 200-hPa geopotential height (shading) and wind (vectors) anomalies in the volcanic period. The ensemble mean of all full-forcing members is shown in (a) and the

ensemble mean of six full-forcing members with stronger cooling is shown in (b). Black vectors indicate wind anomalies significant at the 90% confidence level according to the two-tailed *t* test.

Figure 8. Anomalies of sea surface salinity (units: 10^{-4} PSU) and barotropic stream function (units: Sv) during the periods 1451–1470 CE (a, c) and 1471–1490 CE (b, d). Anomalies are relative to 1432–1451 CE in (a, c) and 1451–1470 CE in (b, d). The subpolar North Atlantic (50°–60°N, 20°–50°W) is outlined by the green box. Areas with significance according to the two-tailed *t* test at the $p < 0.05$ level are stippled.

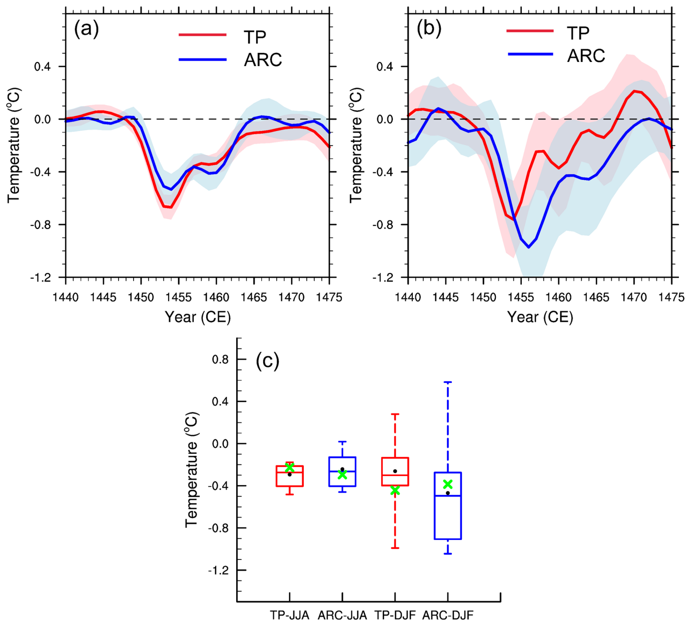
(a)
TP
ARC
Temperature (°C)
0.4
0.0
-0.4
-0.8
-1.2
1440 1445 1450 1455 1460 1465 1470 1475
Year (CE)
(b)
TP
ARC
Temperature (°C)
0.4
0.0
-0.4
-0.8
-1.2
1440 1445 1450 1455 1460 1465 1470 1475
Year (CE)
(c)
Temperature (°C)
0.8
0.4
0.0
-0.4
-0.8
-1.2
TP-JJA
ARC-JJA
TP-DJF
ARC-DJF

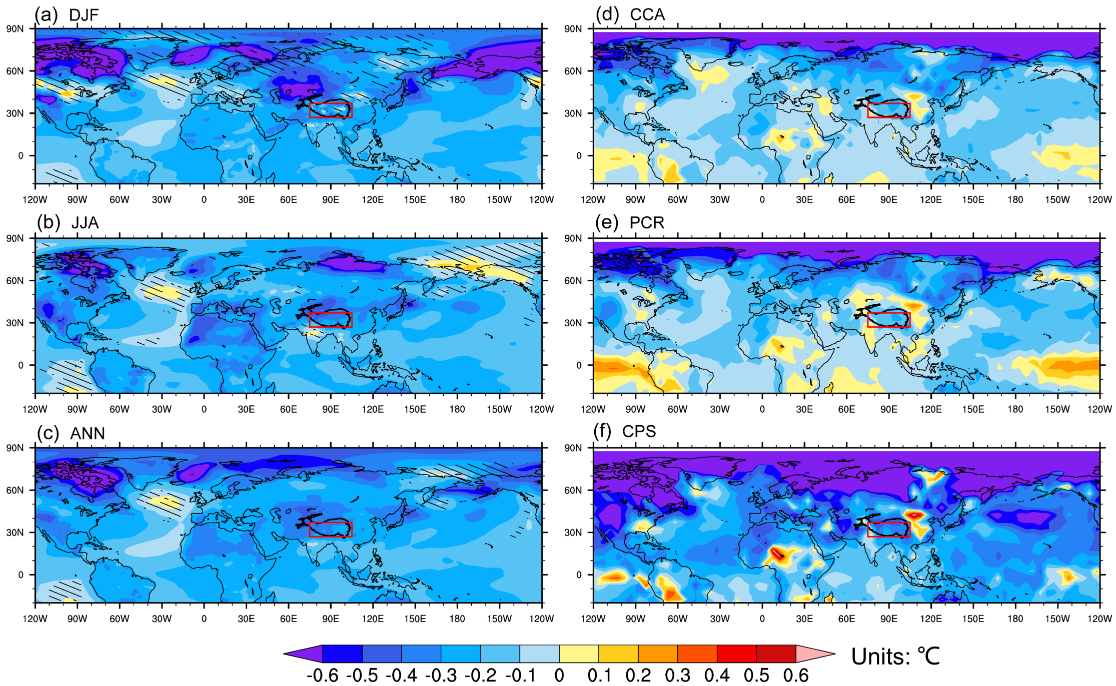
(a) DJF
(b) JJA
(c) ANN
(d) CCA
(e) PCR
(f) CPS
90N
60N
30N
0
120W 90W 60W 30W 0 30E 60E 90E 120E 150E 180 150W 120W
-0.6 -0.5 -0.4 -0.3 -0.2 -0.1 0 0.1 0.2 0.3 0.4 0.5 0.6
Units: ℃

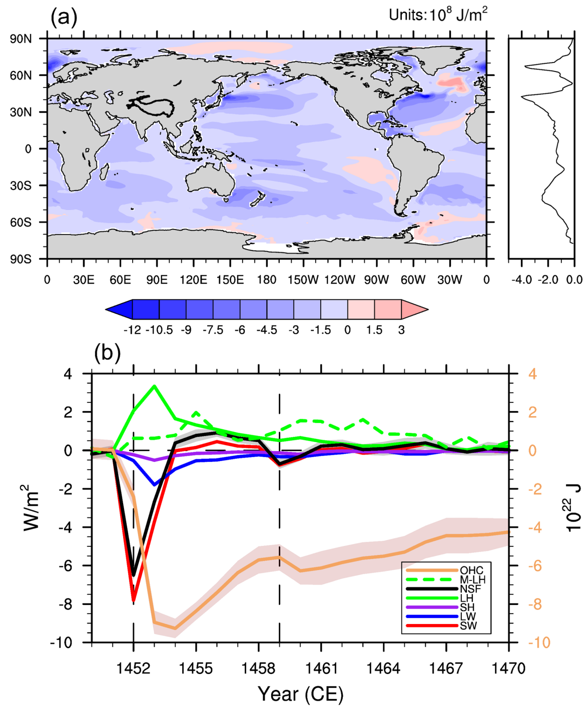
(a)
Units: 10^8 J/m^2
90N
60N
30N
0
30S
60S
90S
0 30E 60E 90E 120E 150E 180 150W 120W 90W 60W 30W 0
-4.0 -2.0 0.0
-12 -10.5 -9 -7.5 -6 -4.5 -3 -1.5 0 1.5 3
(b)
W/m^2
10^22 J
OHC
M-LH
NSF
LH
SH
LW
SW
1452 1455 1458 1461 1464 1467 1470
Year (CE)

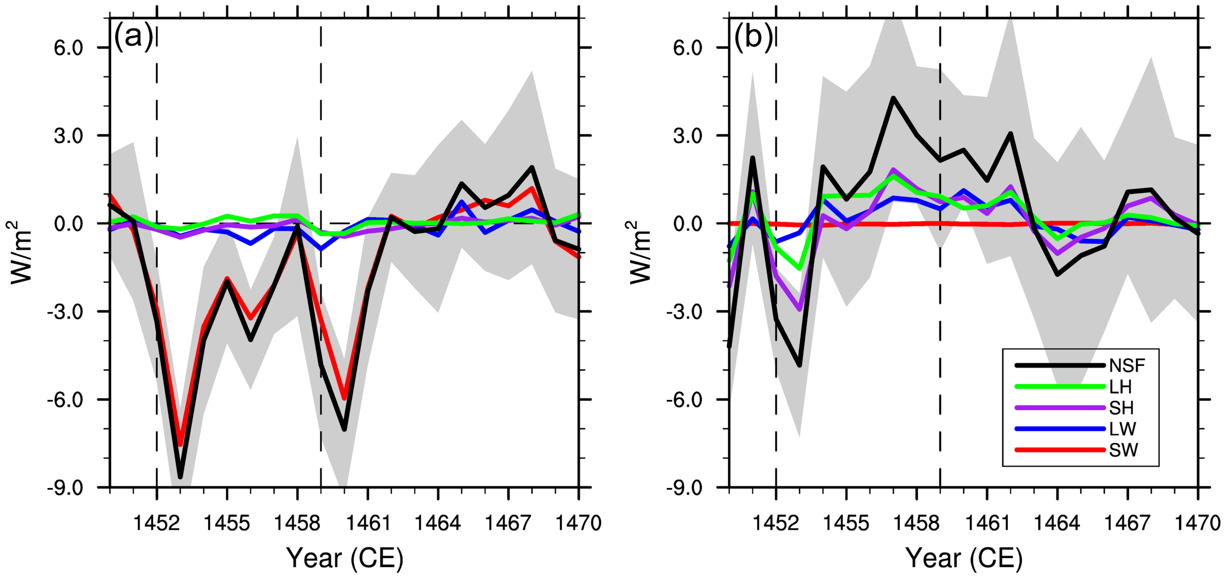
(a)
(b)
6.0
3.0
0.0
-3.0
-6.0
-9.0
W/m2
1452
1455
1458
1461
1464
1467
1470
Year (CE)
NSF
LH
SH
LW
SW

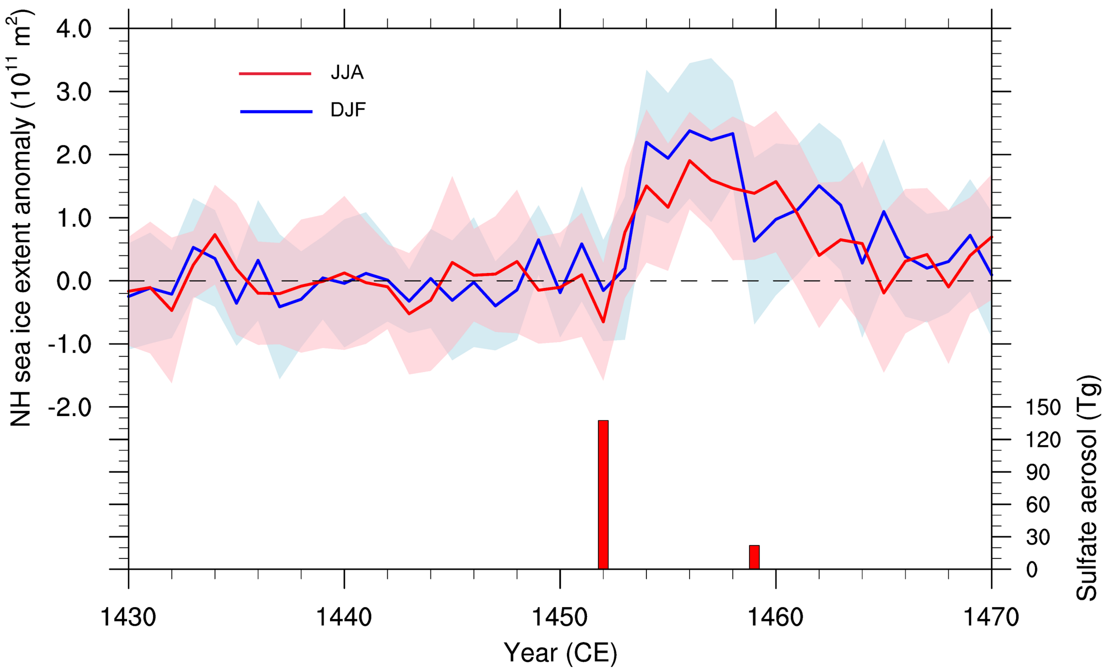
NH sea ice extent anomaly (10^{11} m^2)
4.0
3.0
2.0
1.0
0.0
-1.0
-2.0
JJA
DJF
150
120
90
60
30
0
Sulfate aerosol (Tg)
1430
1440
1450
1460
1470
Year (CE)

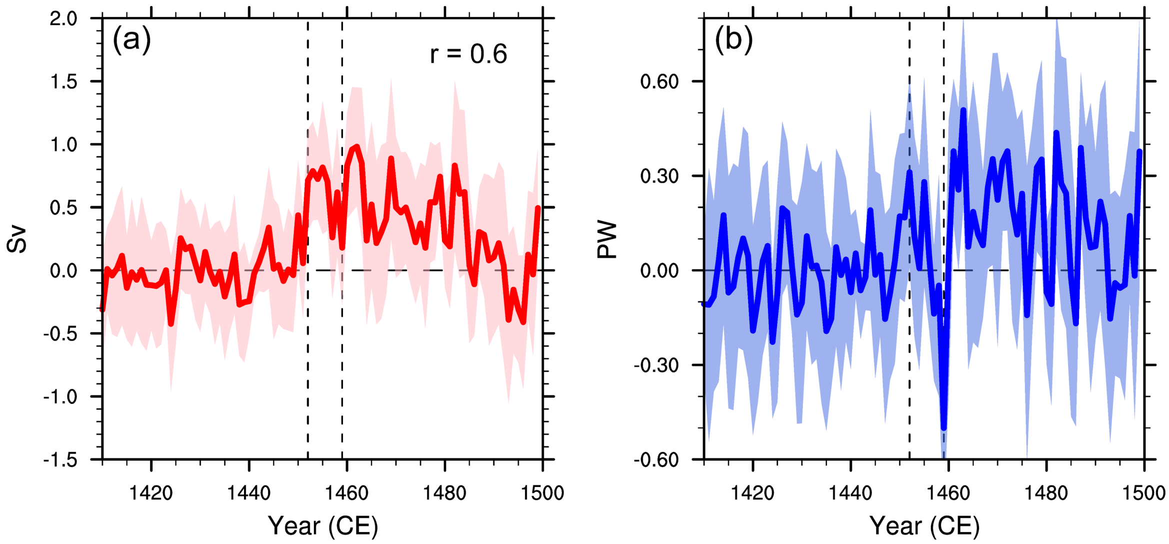

(a)
r = 0.6
Sv
2.0
1.5
1.0
0.5
0.0
-0.5
-1.0
-1.5
1420
1440
1460
1480
1500
Year (CE)
(b)
PW
0.60
0.30
0.00
-0.30
-0.60
1420
1440
1460
1480
1500
Year (CE)

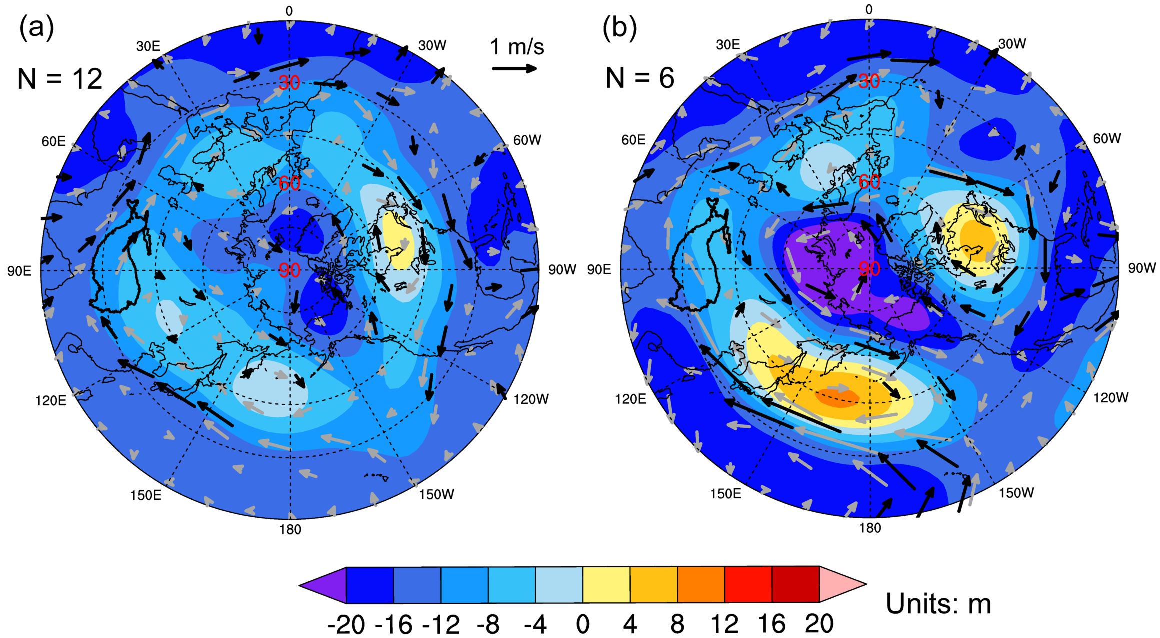
(a)
N = 12
(b)
N = 6
1 m/s
0
30E
30W
60E
60W
90E
90W
120E
120W
150E
150W
180
30
60
90
-20 -16 -12 -8 -4 0 4 8 12 16 20
Units: m

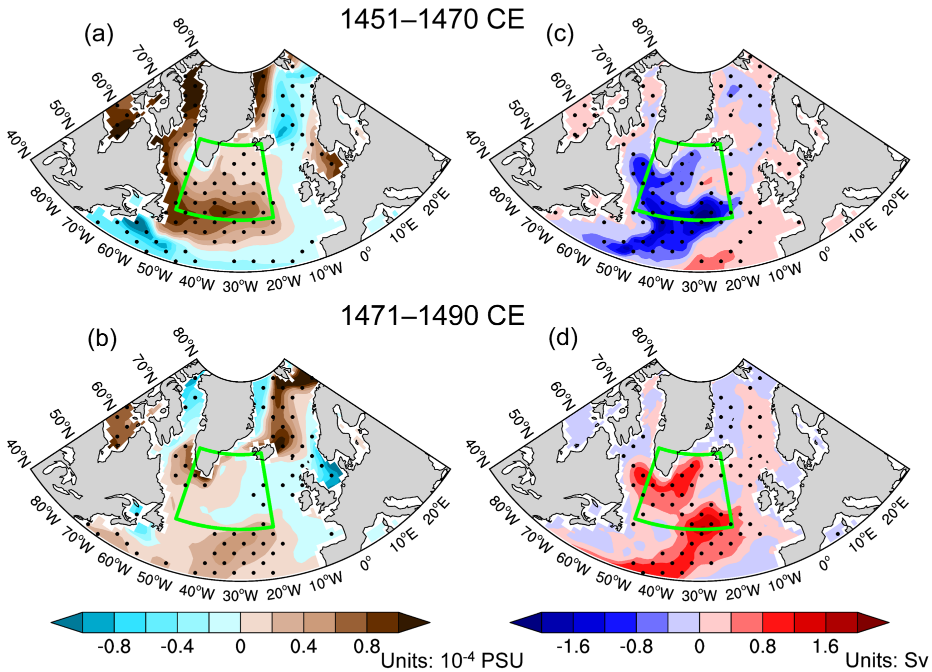
1451–1470 CE
(a)
(c)
1471–1490 CE
(b)
(d)
80°N
70°N
60°N
50°N
40°N
80°W 70°W 60°W 50°W 40°W 30°W 20°W 10°W 0° 10°E 20°E
-0.8 -0.4 0 0.4 0.8
Units: 10-4 PSU
-1.6 -0.8 0 0.8 1.6
Units: Sv